

Control-Aware Trajectory Predictions for Communication-Efficient Drone Swarm Coordination in Cluttered Environments

Longhao Yan, Jingyuan Zhou, and Kaidi Yang

Abstract—Swarms of Unmanned Aerial Vehicles (UAV) have demonstrated enormous potential in many industrial and commercial applications. However, before deploying UAVs in the real world, it is essential to ensure they can operate safely in complex environments, especially with limited communication capabilities. To address this challenge, we propose a control-aware learning-based trajectory prediction algorithm that can enable communication-efficient UAV swarm control in a cluttered environment. Specifically, our proposed algorithm can enable each UAV to predict the planned trajectories of its neighbors in scenarios with various levels of communication capabilities. The predicted planned trajectories will serve as input to a distributed model predictive control (DMPC) approach. The proposed algorithm combines (1) a trajectory compression and reconstruction model based on Variational Auto-Encoder, (2) a trajectory prediction model based on EvolveGCN, a graph convolutional network (GCN) that can handle dynamic graphs, and (3) a KKT-informed training approach that applies the Karush–Kuhn–Tucker (KKT) conditions in the training process to encode DMPC information into the trained neural network. We evaluate our proposed algorithm in a funnel-like environment. Results show that the proposed algorithm outperforms state-of-the-art benchmarks, providing close-to-optimal control performance and robustness to limited communication capabilities and measurement noises.

Index Terms—UAV swarm, collision avoidance, communication-efficient control, trajectory prediction, deep learning

I. INTRODUCTION

A swarm of Unmanned Aerial Vehicles (UAV) refers to a set of aerial robots, such as drones, that fly in a flock to achieve a certain goal. UAV swarms have demonstrated enormous potential in many industrial and commercial applications, such as search and rescue, remote sensing, and construction [3], [23]–[25], [41], [42], [45]. Before the massive deployment of UAV swarms in the real world, it is essential to ensure they can operate safely in complex environments such as cluttered environments where static obstacles and moving agents fill the space in an unorganized manner.

It has been widely demonstrated that decentralized control can coordinate UAV swarms in a safe and efficient manner,

thanks to its benefits in better scalability and reliability [29]–[32], [46]. One category of decentralized control approaches is based on potential fields (PF) that make fast reactive decisions with behavioral rules inspired by biological swarms (e.g., birds and fish) [1], [4]–[6]. Although PF-based approaches have been demonstrated to be efficient, they rarely consider the physical characteristics of UAVs and can yield infeasible or overly conservative decisions, which may not be suitable for cluttered environments with dense obstacles. An alternative category of approaches is based on optimization, e.g., Distributed Model Predictive Control (DMPC), whereby each UAV solves a local optimization model in a decentralized manner to determine its trajectory [9], [11], [27], [28]. Compared to PF-based approaches, optimization-based approaches can explicitly account for physical constraints and generate real-time, collision-free trajectories for UAV swarms in cluttered environments. However, optimization-based approaches typically require UAVs to share planned trajectories with their neighbors at a high frequency to avoid collisions, which heavily relies on reliable communication and may not be robust in scenarios with limited communication capabilities.

Recently, several works have attempted to develop communication-efficient control strategies for UAV swarms and other decentralized multi-robot systems, aiming to reduce communication costs for exchanging state information crucial for decision-making and control [8], [12], [13], [21]. Existing research can be divided into two categories. The first category predicts planned trajectories based on historical states measured by onboard sensors [33]–[36], [38]. For example, [8] developed a learning-based approach based on recurrent neural networks to predict the planned trajectories of each UAV, which does not require communications. However, it is assumed that each UAV can sense the real-time states of all other UAVs, which may not be possible in cluttered environments. The second category seeks to compress the communicated messages on planned trajectories to reduce the bandwidth requirement [37], [39], [40]. For example, [12] proposed a UAV path discretization and compression algorithm that simultaneously optimizes the selection of waypoints and the subpath trajectories while ensuring the optimal performance of trajectory optimization. However, the proposed algorithm only focused on each individual path without exploiting their correlations. Reference [13] developed a neural network-based mean-field approximation approach to approximate the solution to the Hamilton-Jacobi-Bellman (HJB) and Fokker-Planck-Kolmogorov (FPK) equations, which can effectively minimize

The authors are with the Department of Civil and Environmental Engineering, National University of Singapore, Singapore 119077. Email: {longhao.yan, jingyuanzhou}@u.nus.edu, kaidi.yang@nus.edu.sg. *Corresponding author:* Kaidi Yang.

This research was supported by the Temasek Laboratory (TL)@NUS under its Seed Grant (A-0003235-48-00) and by the Singapore Ministry of Education (MOE) under NUS Start-Up Grant (A-8000404-01-00).

This work has been submitted to the IEEE for possible publication. Copyright may be transferred without notice, after which this version may no longer be accessible.

communication. To avoid violating required conditions, this work introduced Federated Learning to enable the sharing of model parameters between UAVs. However, this work requires the online training and sharing of the neural network parameters, which even at low communication frequency, can be a large amount of data to exchange.

From the literature mentioned above, we have identified several research gaps in existing research on communication-efficient UAV swarm coordination. First, existing works either attempt to predict trajectories from historical states or compress communicated messages on planned trajectories but rarely combine both approaches such that these two types of information can compensate for each other. Second, many existing works have made strong assumptions of sensing range or reliable communications and have yet to test their proposed algorithms in scenarios with cluttered environments. Third, existing works rarely consider information about the decision-making process of the UAV swarm, e.g., optimization models, which can be common knowledge for all UAVs in the same swarm. Integrating such knowledge can help ensure that the predicted trajectories are more physically meaningful.

In this paper, we address the aforementioned research gaps by developing a learning-based algorithm that enables each UAV to predict the trajectories of its neighbors in cluttered environments with various levels of communication capabilities. Our algorithm combines three types of information: (i) the historical states of each UAV and its neighbors, (ii) compressed messages communicated from neighbors, if available, and (iii) the information about the decision-making process of each UAV, characterized by a convex optimization-based DMPC approach. The main part of our algorithm combines the first two types of information by integrating two models in a Bayesian framework: a Variational Auto-Encoder (VAE)-based trajectory compression and reconstruction model and a graph convolutional network (GCN)-based trajectory prediction model. Our trajectory prediction model can handle the dynamics scenarios with time-varying swarm alignment, where the neighbors of a given UAV constantly change. This is achieved by leveraging an EvolveGCN architecture [7] that can track the change in the underlying graph. The two models are trained together via a Karush–Kuhn–Tucker (KKT) conditions-informed method [10] to encode the information of the convex optimization model upon which each UAV makes decisions (i.e., the third type of information).

The main contributions of this paper are two-fold. First, we devise a learning-based algorithm to predict the trajectories of surrounding UAVs in cluttered environments with various levels of communication capabilities (bandwidths, packet loss rates, lower frequencies, etc.), which is achieved by combining an EvolveGCN-based trajectory prediction model with a VAE-based trajectory compression and reconstruction model in a Bayesian framework. Second, we train the developed neural network via a KKT-informed approach that enables the trajectory prediction algorithm to encode the information about the decision-making process of UAVs to improve control performance. To the best of our knowledge, no existing trajectory prediction algorithms have explicitly encoded knowledge about the decision-making processes of the agents.

This paper is organized as follows. Section II describes the problem statement, Section III presents our methodology, Section IV presents the simulation settings and results, and Section V concludes the paper.

II. PROBLEM STATEMENT

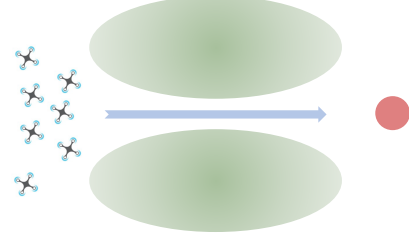


Figure 1: Illustration of the considered scenario, where the red point represents the goal of the swarm, and the green ellipsoids represent the obstacles.

As shown in Figure 1, we consider a swarm of UAVs indexed by $i \in \mathcal{V}$ in a funnel-like environment where the obstacles, indexed by $m \in \mathcal{M}$, are convex and modeled as 3-dimensional ellipsoids, each parameterized by a center point $\mathbf{C}_m \in \mathbb{R}^3$ and an affine transformation matrix $\mathbf{E}_m \in \mathbb{R}^{3 \times 3}$. The considered time horizon is discretized as a set of intervals $\mathcal{K} = \{1, 2, \dots, K\}$ of a given size ΔT indexed by k . The state of UAV $i \in \mathcal{V} = \{1, 2, \dots, n\}$ at time step $k \in \mathcal{K}$ is represented by $\mathbf{x}_i(k) = (\mathbf{p}_i(k), \mathbf{v}_i(k)) \in \mathbb{R}^6$, where $\mathbf{p}_i(k) \in \mathbb{R}^3$ and $\mathbf{v}_i(k) \in \mathbb{R}^3$ denote its location and velocity at time step k , respectively. The dynamics of UAV i can be modeled as a discrete linear system with an underlying position controller:

$$\mathbf{x}_i(k+1) = \mathbf{A}_i \mathbf{x}_i(k) + \mathbf{B}_i \mathbf{u}_i(k) \quad (1)$$

where the control action $\mathbf{u}_i(k)$ represents the desired position at time step k , and \mathbf{A}_i and \mathbf{B}_i are constant matrices.

Each UAV i can collect two types of information: (1) the real-time states of other UAVs within a sensing range, denoted by $\mathbf{x}_j(t)$ for the states of UAV j at time step t , and (2) the messages sent by other UAVs within a communication range, denoted by $\mathbf{z}_j(t)$ for the message sent by UAV j at time step t . For brevity, we assume that the communication graph and the sensing graph are identical, both represented by $\mathcal{G} = (\mathcal{V}, \mathcal{E})$, where edge $e = (i, j) \in \mathcal{E} \subseteq \mathcal{V} \times \mathcal{V}$ indicates that UAV j is within the sensing/communication range of UAV i . Such an assumption is made without loss of generality since the developed algorithm can be extended to distinguish communication and sensing graphs. We further make the following remarks regarding the sensing/communication graph \mathcal{G} . First, we consider such a graph to be dynamic, specifically with a time-invariant node set \mathcal{V} (i.e., fixed swarm) and a time-varying edge set \mathcal{E} (i.e., dynamic neighbors). Such an assumption is realistic since the alignment of UAVs can change dynamically, especially in cluttered environments. Second, the messages sent by UAV j to UAV i can contain possibly compressed information about UAV j 's planned trajectories, which will be used to facilitate the decision-making of UAV i .

Note that the trajectory information is compressed to cater to the limited bandwidth of the communication channel. To simplify the implementation, we assume that each UAV sends identical structured messages to all its neighbors on the communication graph. Nevertheless, this assumption can be easily extended such that UAVs can share customized messages with their neighbors under specific conditions.

The decision-making process of each UAV follows the quadratic programming (QP)-based DMPC approach proposed in [28]. Note that this DMPC-based control algorithm is chosen thanks to its simplicity of implementation. Our proposed trajectory prediction algorithm can also be used with other convex optimization-based decision algorithms.

In the DMPC settings, each UAV $i \in \mathcal{V}$ solves an embedded quadratic programming (QP) problem at each time step k to obtain its decision, i.e., the planned trajectory within the next P time steps denoted as $\mathbf{U}_i^k = \{\mathbf{u}_i(k+h|k)\}_{h=0}^{P-1}$. For each UAV, the input to the QP problem involves (1) its current location and speed, (2) the real-time location information about the obstacles and the UAVs within its neighborhood, and (3) the predicted trajectory of its neighbors in the planning horizon, denoted by $\tilde{\mathbf{U}}_{-i}^k$.

To better formulate collision-avoidance constraints, the planned trajectory of UAV i , \mathbf{U}_i^k , is parameterized by l 3-dimensional Bezier curves of order d , whereby each of these Bezier curves can be uniquely characterized by a set of $d+1$ 3-dimensional control points. Consequently, the planned trajectory \mathbf{U}_i^k is characterized by a vector $\mathbf{w}_i^k \in \mathbb{R}^{3l(d+1)}$ formed by $l(d+1)$ 3-dimensional control points. The relation between the planned trajectory and the control points can be described as $\mathbf{U}_i^k = \mathbf{F}_i \mathbf{w}_i^k$, where \mathbf{F}_i indicates the coefficients of the Bezier curves.

With the aforementioned trajectory parametrization, the embedded QP problem of the DMPC scheme for UAV i can be described in (2)-(8). For brevity, here we provide the general forms and insights of the QP formulation. For the specific derivation of the cost terms and constraint matrices, please refer to [28].

$$\min_{\mathbf{w}_i^k, \epsilon_i^k, \delta_i^k, \zeta_i^k} J_i^k(\mathbf{w}_i^k, \epsilon_i^k, \delta_i^k, \zeta_i^k) \quad (2)$$

$$\text{s.t. } \mathbf{A}_{\text{dyn},i} \mathbf{w}_i^k \leq \mathbf{b}_{\text{dyn},i} \quad (3)$$

$$\mathbf{A}_{\text{cont},i} \mathbf{w}_i^k = \mathbf{b}_{\text{cont},i} \quad (4)$$

$$\begin{aligned} \mathbf{A}_{\text{saf-agent},i}^k \left(\tilde{\mathbf{U}}_{-i}^k \right) \left[(\mathbf{w}_i^k)^T, (\epsilon_i^k)^T \right]^T \\ \leq \mathbf{b}_{\text{saf-agent},i}^k \left(\tilde{\mathbf{U}}_{-i}^k \right) \end{aligned} \quad (5)$$

$$\mathbf{A}_{\text{coh},i}^k \left(\tilde{\mathbf{U}}_{-i}^k \right) \left[(\mathbf{w}_i^k)^T, (\delta_i^k)^T \right]^T \leq \mathbf{b}_{\text{coh},i}^k \left(\tilde{\mathbf{U}}_{-i}^k \right) \quad (6)$$

$$\mathbf{A}_{\text{saf-obs},i}^k \left[(\mathbf{w}_i^k)^T, (\zeta_i^k)^T \right]^T \leq \mathbf{b}_{\text{saf-obs},i}^k \quad (7)$$

$$\epsilon_i^k, \delta_i^k, \zeta_i^k \geq 0 \quad (8)$$

where the objective function is a quadratic function involving (i) migration cost that penalizes the distance to a pre-defined migration point, (ii) inter-agent and agent-obstacle collision costs penalizing the UAV of getting too close to its neighbors and obstacles, (iii) cohesion cost to ensure that adjacent UAVs stay closer than a threshold cohesion distance, and (iv) control

effort cost to minimize the energy spent to execute the control action. Constraint (3) ensures the feasibility of the dynamics given by the planned trajectory parameterized as the Bezier curve. Constraint (4) imposes C^2 -continuity requirement on the derived Bezier curve. Constraints (5) and (6), respectively, indicate the collision avoidance and cohesion between UAV i and its surrounding UAVs to bound the distance between them. Constraint (7) indicates the collision avoidance between UAV i and obstacles. Note that constraints (5)-(7) are linearized from nonlinear constraints and relaxed with relaxation terms ϵ_i^k , δ_i^k , and ζ_i^k minimized in the objective function. Constraint (8) requires these relaxation terms to be nonnegative.

Further note that constraints (5) and (6) depend on the predicted trajectories of the surrounding UAVs, i.e., $\tilde{\mathbf{U}}_{-i}^k$. Hence, the quality of decisions, especially on inter-agent safety and cohesion, heavily depends on the accuracy of such a prediction. Originally in [28], such predictions are assumed to be planned trajectories always available with moderate noises, as they can be obtained through communicating with surrounding UAVs at each time step. However, since the communication channel may have limited bandwidth and frequency, as well as possibility of packet loss, it may not be feasible to share the entire trajectory at each time step. Therefore, it is important to develop a communication-efficient and robust method for trajectory prediction, which will be developed in Section III.

III. CONTROL-AWARE LEARNING-BASED TRAJECTORY PREDICTION

To address the challenge imposed by limited communication, we devise a learning-based approach to predict the trajectories of surrounding UAVs of each UAV $i \in \mathcal{V}$. Here, we seek to predict the trajectories of surrounding UAVs by estimating their planned trajectories at the previous time step. The reason is three-fold. First, due to embedded motion control modules in UAVs, we envision the planned trajectory to be close to the actual trajectory, especially if the planning horizon is relatively short. Second, the estimation of the planned trajectories enables us to encode more physical information (e.g., the decision-making process of UAVs) and thus can be more sample efficient in training. Third, using the planned trajectories to represent future trajectories is commonly seen in existing literature [8], [28], [33], [43], [44], which enables us to better integrate our approach with state-of-the-art control algorithms. Mathematically, let $\tilde{\mathbf{U}}_{ij}^{k-1}$ be the planned trajectory of UAV j calculated at time step $k-1$ and estimated by UAV i at the beginning of time step k . For brevity, We simplify the notion $\tilde{\mathbf{U}}_{ij}^{k-1}$ to $\tilde{\mathbf{U}}_j^{k-1}$ by omitting i if there is no ambiguity. Hence, the predicted trajectory of all neighbors of UAV i , $\tilde{\mathbf{U}}_{-i}^k$, can be represented by $\tilde{\mathbf{U}}_{-i}^k = \{\tilde{\mathbf{U}}_j^{k-1}\}_{j \in \mathcal{N}_i}$.

The proposed trajectory prediction approach involves four components as illustrated in Figure 2: (i) a Variational Auto-Encoder (VAE)-based component that allows each UAV to compress its planned trajectory and reconstruct the compressed messages sent by other UAVs, (ii) an EvolveGCN (EG)-based trajectory prediction component for the estimation of the planned trajectory in scenarios with dynamic sensing/communication graphs, (iii) a Bayesian layer to integrate

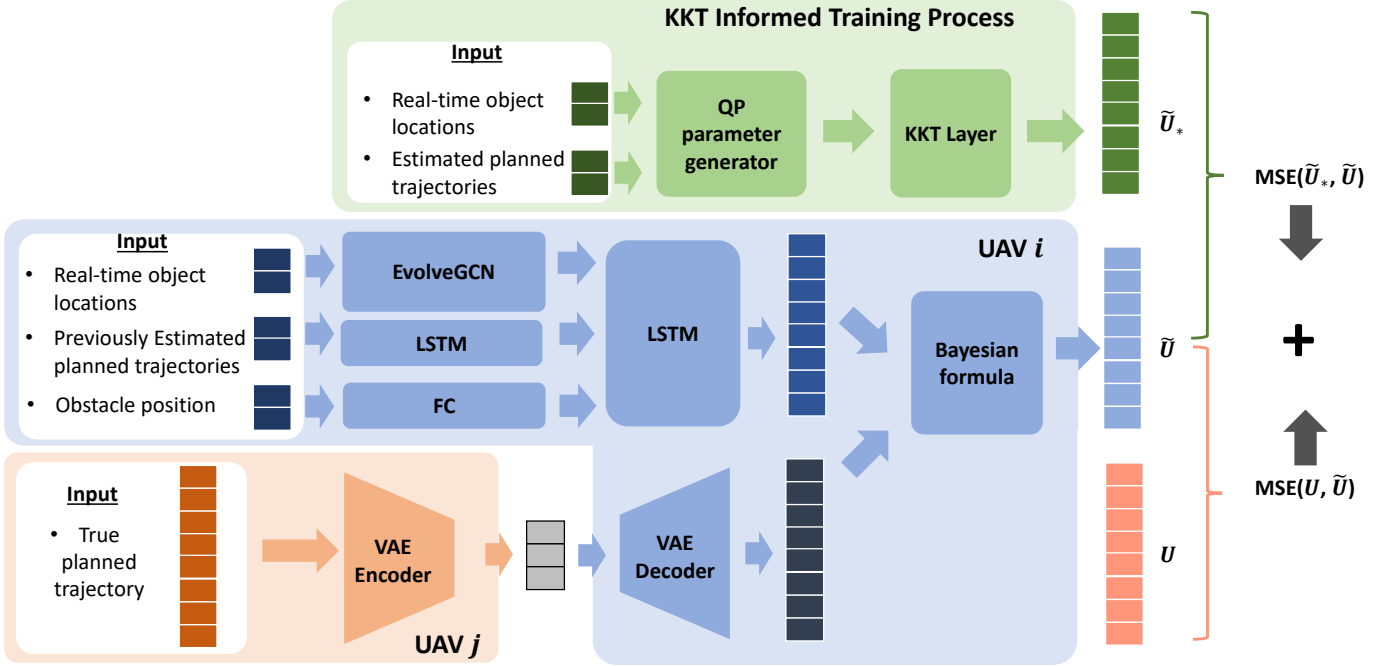


Figure 2: Framework of the trajectory prediction algorithm

the reconstructed planned trajectories by VAE and the estimated planned trajectories by the trajectory prediction component, and (iv) a KKT-enhanced training approach that devises a KKT-based differential layer to encode the structural information of the embedded QP into the trained neural network. The details of these components are detailed below in Sections III-A–III-D. Note that the developed learning-based model is implemented in each UAV with identical parameters.

A. VAE for trajectory compression and reconstruction

A VAE is designed for trajectory compression and reconstruction, which consists of an encoder ϕ_e and a decoder ϕ_d . The encoder is leveraged by UAV $j \in \mathcal{N}_i$ to compress its planned trajectory $\mathbf{U}_j^{k-1} \in \mathbb{R}^{3P}$ into a low-dimensional message $\mathbf{z}_j^k \in \mathbb{R}^L$ ($L < 3P$). Specifically, the encoder is implemented as a neural network that outputs a vector of means $\phi_e(\mathbf{U}_j^{k-1}) \in \mathbb{R}^L$ and standard deviations $\boldsymbol{\eta}_j^k \in \mathbb{R}^L$ of independent Gaussian distributions, from which the message \mathbf{z}_j^k is sampled and transmitted to UAV i . After UAV i receives the message \mathbf{z}_j^k , it uses the decoder to reconstruct an estimated planned trajectory $\tilde{\mathbf{U}}_{j,\text{VAE}}^{k-1} = \phi_d(\mathbf{z}_j^k)$. In this paper, both the encoder network ϕ_e and decoder network ϕ_d are implemented as fully-connected layers. In addition, the trajectory reconstructed by the decoder naturally makes VAE an estimator of the true trajectory.

B. EvolveGCN (EG)-based trajectory prediction

Our EvolveGCN (EG)-based trajectory prediction component enables UAV i to estimate the planned trajectories of all its neighbors, $\tilde{\mathbf{U}}_{j,\text{EG}}^{k-1}$, leveraging (i) the geometric information of obstacles and (ii) the location information within a horizon of H past time steps $\mathbf{p}^{k,\text{hist}} = \{\mathbf{p}_j^{k-h}\}_{j \in \mathcal{N}_i, h \in \{0,1,\dots,H\}}$ of

surrounding UAVs, measured by the onboard sensors of UAV i , and (iii) the planned trajectories of UAV $\tilde{\mathbf{U}}_j^{k-2}$ estimated at the previous time step $k-1$.

As shown in Figure 2, the overall architecture involves four parts: (i) a Long Short-Term Memory (LSTM)-based encoder to characterize the correlations between planned trajectories estimated at consecutive time steps, (ii) an obstacle encoder to extract the geometric features of obstacles, (iii) an EvolveGCN layer [7] to extract the spatiotemporal correlations of UAVs on the dynamic sensing graph, and (iv) an LSTM-based decoder to generate estimated $\tilde{\mathbf{U}}_{j,\text{EG}}^{k-1}$ and its standard deviation $\boldsymbol{\sigma}_{j,\text{EG}}^k$. Parts (i), (ii), and (iv) build on the trajectory planning neural network developed in [8] and extend it by allowing a probabilistic output representation for the integration with VAE reconstruction outcomes. Moreover, unlike [8] that requires each UAV to measure the real-time locations of all other UAVs, we consider a dynamic sensing graph evolving with the movement of the swarm to capture the topological information of the UAV swarm. To this end, we add Part (iii) with an EvolveGCN (EG) architecture, which represents the swarm alignment by a graph convolutional network (GCN) and evolves its parameters along the temporal dimension using LSTM without resorting to node embeddings.

The details of the four parts are described as follows.

(i) *LSTM-based encoder*. An LSTM layer is leveraged to exploit the temporal correlations between the planned trajectories of UAV j at consecutive time steps. This encoder can be mathematically represented as:

$$\mathbf{y}_j^k = \text{LSTM}_{\text{query}}\left(\tilde{\mathbf{U}}_j^{k-2}\right), \quad j \in \mathcal{N}_i \quad (9)$$

where the output \mathbf{y}_j^k serves as an input to the LSTM decoder, i.e., Part (iv).

(ii) *Obstacle encoder*. Since we only consider static obstacles, we design the obstacle encoder as a fully connected layer with an input of the parameters characterizing the obstacles. This encoder can be mathematically represented as:

$$\mathbf{o}^k = \text{FC}_{\text{obs}}(\mathbf{C}_m), \quad m \in M \quad (10)$$

where the output \mathbf{o}^k serves as an input to the LSTM decoder, i.e., Part (iv).

(iii) *EG layers*. As mentioned above, the EG layers are adopted to extract the spatiotemporal correlations of UAVs in time-varying sensing graphs. The input to the EG layers includes the position information of H past time steps $\mathbf{p}^{k,\text{hist}}$ within the sensing range of UAV i . The output of the EG layers, \mathbf{g}^k , serves as an input to the LSTM decoder, i.e., Part (iv).

Each EG layer involves a GCN layer and an LSTM layer, whereby the GCN layer captures the topology of the sensing graph seen by UAV i , represented as adjacency matrix $\mathbf{G}_i^k \in \mathbb{R}^{n \times n}$, where the elements involving unseen UAVs are set to zero. The LSTM layer is employed to model the evolution of the GCN weight matrix as a dynamical system. Specifically, let $\mathbf{W}^{k,(l)}$ denote the dynamic GCN weight matrix of the l -th layer at time step k , and $\mathbf{H}^{k,(l)}$ represents the node embeddings of the l -th layer at time step k . The EG layer can be written as:

$$\mathbf{H}^{k+1,(l+1)} = \text{GCONV}(\mathbf{G}_i^k, \mathbf{H}^{k,(l)}, \mathbf{W}^{k,(l)}) \quad (11)$$

$$\mathbf{W}^{k+1,(l)} = \text{LSTM}_{\text{eg}}(\mathbf{W}^{k,(l)}). \quad (12)$$

where the initial embedding matrix $\mathbf{H}^{k,(0)}$ includes the node features as the output of the LSTM-based encoder (i.e., \mathbf{y}^k), and the final embedding matrix $\mathbf{H}^{k,(L)}$ is the output of the EG layer (i.e., \mathbf{g}^k). The activation function $\pi(\cdot)$ is chosen as ReLU for all but output layers and an identity function for the output layer.

In (12), the evolution of the weight matrix $\mathbf{W}^{k,(l)}$ is solely based on the weight matrix at the previous time step, which is referred to as EGCU-O. An alternative way of formulating this LSTM layer is to incorporate node embeddings $\mathbf{H}^{k,(l)}$, i.e., $\mathbf{W}^{k+1,(l)} = \text{LSTM}(\mathbf{H}^{k+1,(l)}, \mathbf{W}^{k,(l)})$, referred to as EGCU-H [7]. In this paper, we use EGCU-O for its simplicity.

(iv) *LSTM-based decoder*. The decoder synthesizes the outputs of the LSTM encoder, the obstacle encoder and the EG layer with an LSTM layer followed by a fully connected layer to generate the sequence of estimated planned trajectories of UAV j , $\tilde{\mathbf{U}}_j^{k-1}$, which can be written as:

$$\tilde{\mathbf{U}}_{j,\text{EG}}^{k-1}, \sigma_{j,\text{EG}}^{k-1} = \text{Decoder}_{\text{LSTM}}(\mathbf{y}_j^k, \mathbf{o}^k, \mathbf{g}^k) \quad (13)$$

where the distribution of the planned trajectories is given as a Gaussian distribution with mean $\tilde{\mathbf{U}}_{j,\text{EG}}^{k-1}$ and covariance matrix $\Sigma_{j,\text{EG}}^{k-1} = \left(\text{diag}(\sigma_{j,\text{EG}}^{k-1})\right)^2$. We choose the covariance matrix as a diagonal matrix, a typical treatment in existing works to simplify the underlying neural network.

C. Bayesian integration of predicted planned trajectories

Note that both the VAE and EG-based trajectory prediction components provide an estimation of the planned trajectories.

The aim of this component is to combine them via a simple Bayesian approach. Specifically, we treat the outcome of the trajectory prediction module as the prior, because such estimation will always be available despite communication failure. Specifically, the prior distribution is characterized by a Gaussian distribution written as:

$$\mathbf{U}_j^{k-1} | \tilde{\mathbf{U}}_{j,\text{EG}}^{k-1} \sim N\left(\tilde{\mathbf{U}}_{j,\text{EG}}^{k-1}, \Sigma_{j,\text{EG}}^{k-1}\right) \quad (14)$$

where \mathbf{U}_j^{k-1} represents the true planned trajectories made by UAV j at time step $k-1$.

If UAV i receives a message \mathbf{z}_j from UAV j and reconstructs it, the reconstructed outcome, $\tilde{\mathbf{U}}_{j,\text{VAE}}^{k-1}$, will serve as an observation, i.e.,

$$\tilde{\mathbf{U}}_{j,\text{VAE}}^{k-1} | \mathbf{U}_j^{k-1} \sim N\left(\mathbf{U}_j^{k-1}, \Sigma_{\text{VAE}}^{k-1}\right), \quad j \in \mathcal{N}_i \quad (15)$$

where the covariance matrix $\Sigma_{\text{VAE}}^{k-1}$ can be obtained empirically from a well-trained VAE.

Combining (14) and (15), the posterior distribution can be derived using the Bayesian formula as in Eq.(16). Here, notice that $\tilde{\mathbf{U}}_{j,\text{VAE}}^{k-1}$ and $\tilde{\mathbf{U}}_{j,\text{EG}}^{k-1}$ are independent.

$$p(\mathbf{U}_j^{k-1} | \tilde{\mathbf{U}}_{j,\text{VAE}}^{k-1}, \tilde{\mathbf{U}}_{j,\text{EG}}^{k-1}) \propto p(\mathbf{U}_j^{k-1} | \tilde{\mathbf{U}}_{j,\text{EG}}^{k-1}) p(\tilde{\mathbf{U}}_{j,\text{VAE}}^{k-1} | \mathbf{U}_j^{k-1}). \quad (16)$$

The final estimation can be calculated via maximum a posteriori (MAP) as $\tilde{\mathbf{U}}_j^{k-1} = \arg \max_{\mathbf{U}_j^{k-1}} p(\mathbf{U}_j^{k-1} | \tilde{\mathbf{U}}_{j,\text{VAE}}^{k-1}, \tilde{\mathbf{U}}_{j,\text{EG}}^{k-1})$.

D. KKT-informed training of the trajectory prediction neural network

Sections III-A – III-C jointly define a learning-based framework for trajectory prediction with a neural network model. This neural network is trained with data generated from simulations. For details about the generation of training data used in this paper, please refer to Section IV-B. One classical method to train the neural network is to minimize the l_2 -loss, written as

$$\mathcal{L}_2(\tilde{\mathbf{U}}_j^{k-1}, \mathbf{U}_j^{k-1}) = \|\tilde{\mathbf{U}}_j^{k-1} - \mathbf{U}_j^{k-1}\|_2^2 \quad (17)$$

where \mathcal{L}_2 represents the l_2 -loss function.

Although such a classical method is widely used, it has two drawbacks. First, it cannot ensure that the estimated planned trajectories serve as a solution to the embedded QP model of DMPC, e.g., whether they satisfy the constraints or can minimize costs. This may lead to estimation errors that can be detrimental to the control performance. Second, this classical method ignores the structural information of the DMPC model, which can be helpful for the training of the neural network. Since UAVs use the same DMPC model, they know perfectly the dynamics and decision processes of other UAVs. Specifically, if UAV i knows all the input of UAV j to the DMPC model, UAV i can accurately obtain the planned trajectories of UAV j simply by solving the DMPC model with UAV j 's input.

We will address these two drawbacks by employing a KKT-informed training approach that brings information about the DMPC to the training process. The structure of the training process is illustrated in Figure 2, which involves two parts: (i) a QP generation neural network that generates the parameters

of the embedded QP of the DMPC approach and (ii) a differentiable KKT layer for solving QP and backpropagating the gradients.

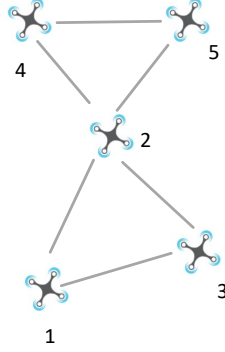


Figure 3: Example for QP parameter estimation. UAV 1 wants to estimate the planned trajectories of UAV 2, which solves a QP using information about UAVs 3, 4, and 5. Note that UAV 1 can sense the real-time states of UAV 3 but not UAVs 4 and 5. To reconstruct the QP model solved by UAV 2, UAV 1 already has the information about itself and UAV 3 but needs to estimate the parameters of UAV 4 and UAV 5. Further note that in general cases, UAV 1 may not know the number of UAVs that influence the decision-making of UAV 2 (e.g., there could be UAV 6, 7, etc.).

(i) *QP generation neural network.* This part aims to enable UAV i to estimate the QP parameters to approximate the DMPC model solved by UAV j , in particular the QP parameters associated with UAVs beyond the sensing range of UAV i . One example is illustrated in Figure 3. To simplify the estimation problem, our QP generation neural network assumes that around each UAV, there are 4 dummy UAVs imposing a significant impact on its decisions. The number 4 is chosen to be the minimum number that can define a 3-dimensional polygon with these UAVs at vertices. The input to the neural network includes the real-time and historical locations $\{\mathbf{p}_{j'}^{k-h}\}_{h=0}^H$ of UAV j and its neighbors and obstacles sensed by UAV i , along with the estimated planned trajectory produced by either VAE or the EG-based trajectory predictor. The output of the neural network includes the estimated parameters of the QP solved by UAV j , which are characterized by the planned trajectories of 4 dummy UAVs at time step $k-1$. The neural network architecture is defined as an EG layer along with fully connected layers.

(2) *Differentiable KKT layer.* With the estimated QP parameters of UAV j , UAV i can solve the QP of UAV j and obtain a primal solution $\tilde{\mathbf{U}}_{*,j}^{k-1}$ and a dual solution $\tilde{\boldsymbol{\lambda}}_{*,j}^{k-1}$. We will then use these solutions to inform the training of the network parameters. Specifically, the loss function can be written as

$$\mathcal{L}_{\text{KKT}}(\tilde{\mathbf{U}}_j^{k-1}, \mathbf{U}_j^{k-1}) = \alpha \|\tilde{\mathbf{U}}_j^{k-1} - \mathbf{U}_j^{k-1}\|_2^2 + \beta \|\tilde{\mathbf{U}}_{*,j}^{k-1} - \mathbf{U}_j^{k-1}\|_2^2 \quad (18)$$

where the first term aims to minimize the mean square error between the true (i.e., \mathbf{U}_j^{k-1}) and estimated values of the planned trajectories produced by VAE and/or the EG-based

trajectory predictor (i.e., $\tilde{\mathbf{U}}_j^{k-1}$), and the second term aims to minimize the mean square error between the true trajectory (i.e., \mathbf{U}_j^{k-1}) and QP solution ($\tilde{\mathbf{U}}_{*,j}^{k-1}$).

When calculating the gradient of the loss function with respect to the neural network parameters, we need to backpropagate the gradient information of the primal and dual solutions. Specifically, these derivatives are found using Proposition 1, which performs sensitivity analysis on the KKT conditions.

Proposition 1 (Differentiable KKT Layer [10]). *Given primal solution \mathbf{w}^* and dual solution $\boldsymbol{\lambda}^*$ to the following QP*

$$\min_{\mathbf{w}} \quad \frac{1}{2} \mathbf{w}^T \mathbf{Q}(\mathbf{u}) \mathbf{w} + \mathbf{q}(\mathbf{u})^T \mathbf{w} \quad (19)$$

$$\mathbf{R}(\mathbf{u}) \mathbf{w} \leq \mathbf{b}(\mathbf{u}) \quad (20)$$

where the parameters are functions with respect to parameters \mathbf{u} . Then the derivatives of the primal and dual solutions $(\frac{\partial \mathbf{w}^*}{\partial \mathbf{u}}, \frac{\partial \boldsymbol{\lambda}^*}{\partial \mathbf{u}})$ satisfy

$$\mathbf{Q} \frac{\partial \mathbf{w}^*}{\partial \mathbf{u}} + \frac{\partial \mathbf{Q}}{\partial \mathbf{u}} \mathbf{w}^* + \frac{\partial \mathbf{q}}{\partial \mathbf{u}} + \mathbf{R} \frac{\partial \boldsymbol{\lambda}^*}{\partial \mathbf{u}} + \frac{\partial \mathbf{R}}{\partial \mathbf{u}} \boldsymbol{\lambda}^* = \mathbf{0} \quad (21)$$

$$\left(\frac{\partial \boldsymbol{\lambda}^*}{\partial \mathbf{u}} \right)^T (\mathbf{R} \mathbf{w}^* - \mathbf{b}) + (\boldsymbol{\lambda}^*)^T \left(\frac{\partial \mathbf{R}}{\partial \mathbf{u}} \mathbf{w}^* + \mathbf{R} \frac{\partial \mathbf{w}^*}{\partial \mathbf{u}} - \frac{\partial \mathbf{b}}{\partial \mathbf{u}} \right) = 0 \quad (22)$$

Notice that the KKT layer is only used to facilitate the training of the trajectory prediction network instead of as another estimator. This is because the forward propagation of the KKT layer requires solving a sequence of QPs, which can be computationally expensive for real-time implementation. Nevertheless, minimizing the loss function $\mathcal{L}_{\text{KKT}}(\cdot)$ can incorporate the structural information of the QP model into the trained neural network. Hence, this treatment is expected to improve the prediction accuracy.

IV. SIMULATION AND ANALYSIS

In this section, we perform simulations to evaluate the proposed trajectory prediction algorithm in a typical funnel-like environment. We first introduce the benchmark algorithms utilized in the simulations in Section IV-A. Then the scenario generation process and parameters are given in Section IV-B. We next analyze the simulation results, including the comparison of the proposed method with other benchmark algorithms (Section IV-C), the robustness in scenarios with limited communication capabilities (Section IV-D), and the sensitivity to measurement noises (Section IV-E).

A. Benchmarks

We evaluate our proposed trajectory prediction algorithm by comparing it to the following benchmarks. These seven benchmark algorithms are chosen to evaluate the value of each component of the proposed algorithm.

- **Baseline.** The baseline algorithm follows [8]. The input to the algorithm is the real-time and historical location information of all UAVs in the swarm, as well as geometric information about the static obstacles. Notice that this algorithm does not consider the dynamic nature of the

UAV alignment. The architecture of the baseline algorithm includes an LSTM-based encoder and an LSTM-based decoder.

- VAE only. This benchmark only has the VAE component, where each UAV uses the decoder to reconstruct the compressed messages without integrating the real-time information about surrounding UAVs. This benchmark is trained by minimizing the l_2 loss.
- EG only. This benchmark only involves the EvolveGCN-based trajectory prediction component that uses real-time and historical location information about the surrounding UAVs to estimate their planned trajectories. This benchmark corresponds to the scenario where communication is not available. This benchmark is trained by minimizing the l_2 loss. The comparison between EG and Baseline shows the value of considering the topological information about the UAV swarm.
- VAE + EG (Bayesian). This benchmark assumes the availability of both VAE and the EvolveGCN-based trajectory prediction components, and uses the Bayesian formula to fuse the estimation outcomes. This benchmark is trained by minimizing the l_2 loss. The comparison between VAE and VAE+EG (Bayesian) shows the value of real-time sensing, and the comparison between EG and VAE+EG (Bayesian) shows the value of communication.
- VAE + KKT. This benchmark evaluates the estimation performance of the VAE component with the aid of the KKT-informed component, where the KKT-informed component is only activated during the training process due to its forward computational complexity.
- VAE + EG + KKT. The only difference between this benchmark and VAE + EG (Bayesian) is that this benchmark is trained with the differential KKT layer. This benchmark is further evaluated under scenarios with various compression levels, communication frequencies, and packet loss rates. The comparison between VAE + EG + KKT and VAE+EG shows the value of the differentiable KKT layer in the training of the model.
- DMPC. This benchmark assumes perfect communication between agents and hence is treated as the oracle. The resulting planned trajectories are regarded as ground truths.

B. Implementation Details

We randomly generate simulation scenarios for training and testing the proposed trajectory prediction algorithm. Specifically, each scenario simulates the dynamics of a UAV swarm in a 3-dimensional funnel-like environment with two obstacles modeled as ellipsoids. The centers of these ellipsoids are sampled uniformly at random from cubes $\mathcal{C}_1 = \{(p_x, p_y, p_z) | p_x \in [10, 14], p_y \in [3.5, 4.5], p_z \in [-2, 2]\}$ and $\mathcal{C}_2 = \{(p_x, p_y, p_z) | p_x \in [10, 14], p_y \in [-3.5, -4.5], p_z \in [-2, 2]\}$, where the values are in meters. The lengths of the three axes of the ellipsoids are sampled uniformly at random from $\{(r_x, r_y, r_z) | r_x \in [4, 8], r_y \in [3, 4], r_z \in [4, 8]\}$ (in meters). We further enforce the minimum distance between these two ellipsoids to range between 0.6 m and 1.2 m by removing the scenarios that violate this condition.

The swarm size is sampled uniformly at random from set $N = \{n \in \mathbb{Z} | 6 \leq n \leq 14\}$. The initial locations of the UAVs are generated within a space $\{(p_x, p_y, p_z) | p_x \in [0, 3], p_y \in [-4, 4], p_z \in [-1, 1]\}$ (in meters) using the Poisson Disk Sampling approach, which ensures that the distance between any pair of UAVs is above a minimum Euclidean distance of 0.7 m. The minimum, maximum, and desired velocities of each UAV are assumed to be -1.5 m/s, 1.5 m/s, and 0.5 m/s, respectively. The minimum and maximum acceleration rates are assumed to be -1 m/s² and 1 m/s², respectively. We aim to prevent collisions between UAV i and other UAVs/obstacles by requiring $\|\mathbf{p}_i - \mathbf{p}\|_{\mathbf{E}} \geq r_{\min}$, where \mathbf{E} represents a linear transformation matrix, \mathbf{p}_i represents the location of UAV i , \mathbf{p} represents the location of another UAV or the closest point of an obstacle, and r_{\min} represents a safety buffer chosen as $r_{\min} = 0.15$ m. If $\|\mathbf{p}_i(k) - \mathbf{p}(k)\|_{\mathbf{E}} < r_{\text{coll}}$, we say that collisions occur, where the collision threshold r_{coll} is chosen as 0.07 m.

The dynamics of the UAV swarm follow (1) with the control input determined using the DMPC module, where the system matrices of the UAVs (i.e., \mathbf{A}_i and \mathbf{B}_i) follow the dynamics of the Crazyflie 2.1 quadrotor with an underlying position controller. The sampling time and DMPC planning horizon are $\Delta T = 0.2$ s and $P = 16$, respectively. The UAV trajectories within each planning horizon are parameterized as $l = 3$ Bezier curves with order $d = 5$. For each scenario, we perform a simulation for $T = 30$ s. Following [28], we consider Gaussian position measurement noises with zero mean and a default standard deviation of 0.004 m, which will be increased in the testing phase to evaluate the algorithm's robustness.

We generate the training dataset by randomly generating 300 simulation scenarios according to the aforementioned distributions. Within each scenario, we collect the following information: (1) real-time locations and velocities of each UAV, (2) the location of obstacles, and (3) the QP matrices and solutions of each UAV at each time step. In total, we collected 450,000 samples, which were then transformed into the training data of the neural networks. Note that the training dataset is generated with the benchmark DMPC, meaning that we assume perfect communication channels such that the input to the QP models is always available and accurate.

The experiments are conducted on a computer with an Intel i7-12700 CPU@2.10 GHz and an NVIDIA RTX 3070 GPU. The designed learning networks are implemented in Python using Pytorch 1.13.1. The DMPC control scheme is implemented on MATLAB R2022b. The input size of the VAE module is 16, consistent with the prediction horizon P . The input size for all EG modules and LSTM encoder modules is 20, which is the horizon length for UAV past state observation H . All hidden layers in the neural network have 128 neurons and the output layer of different modules are all set to be 16. ReLu is selected to be the activate function and all the neural networks are trained under a learning rate of 0.0001.

C. Performance in testing scenarios

In this subsection, we show the results of the testing scenarios. Specifically, we generate another set of 50 scenarios

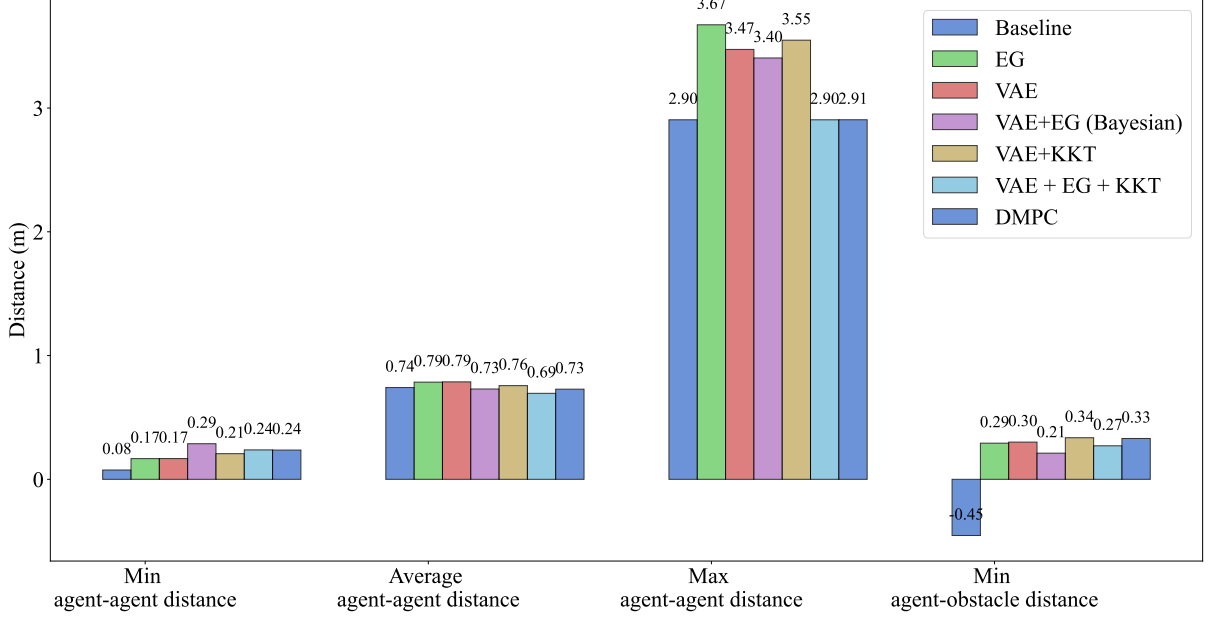


Figure 4: Distance comparison between different algorithms.

for testing, according to the scenario distribution described in Section IV-B. For each testing scenario, we are interested in analyzing control performance and prediction performance. To evaluate control performance, we measure two key factors for each benchmark algorithm: the total incurred cost throughout the simulation period for efficiency and the distances between agents as well as between agents and obstacles for safety. We will further evaluate our algorithm in various scenarios with different parameters to show the robustness of our algorithms in less ideal cases. The data compression levels of VAE, i.e., the latent dimension, range from $L = 6$ to $L = 42$. Notice that the original dimension of the planned trajectories is $L = 48$. The communication frequencies range from $f_{\text{comm}} = 5$ Hz to $f_{\text{comm}} = 1.25$ Hz. The packet loss rates are set to range from $P_{\text{loss}} = 0$ to $P_{\text{loss}} = 1/2$, and the measurement noise levels range from 0 to 0.032. For prediction performance, we will evaluate the mean square errors (MSE) of the predicted planned trajectories compared to the ground-truth planned trajectories solved by DMPC.

Table I: Cost comparison between different algorithms

Algorithm	Safe-Agent Cost	Safe-Obs Cost	Control Effort	Cohesion Cost	Total Cost
Baseline	5444	63793	116711	45018	230966
EG	0	0	158302	187283	345586
VAE	0	0	146930	173067	319997
VAE + EG (Bayesian)	0	0	191507	107096	298603
VAE + KKT	0	0	186482	109678	296160
VAE + EG + KKT	0	0	159758	51027	210786
DMPC	0	0	141084	67298	208382

We first compare the performance of the benchmarks listed in Section IV-A with all parameters set to the default values, i.e., $L = 24$, $f_{\text{comm}} = 5$ Hz, $P_{\text{loss}} = 0$, and measurement noise level 0.004 m. The resulting average control costs across all scenarios are summarized in Table I, whereby the Safe-Agent Cost penalizes the violation of the safety constraints between UAVs, the Safe-Agent Obs Cost penalizes the violation of the safety constraints between UAVs and obstacles, the Control Effort cost helps to minimize the energy spent to execute the control action, the Cohesion Cost penalizes UAVs being too far away from each other, and the total cost is the sum of all four costs. Figure 4 illustrates agent-agent and agent-obstacle distances, averaged over all testing scenarios, whereas the temporal evolution of these distances in a typical scenario is illustrated in Figures 5 – 11. To better understand the control performance, we further summarize the average trajectory prediction errors (in terms of MSE) across all testing scenarios in Tables II – IV.

Performance of the proposed algorithm. From Table I and Figure 4, we can see that the proposed trajectory prediction algorithm VAE+EG+KKT ensures safety and yields similar control performance to DMPC, outperforming other benchmarks. This can be further elaborated by looking at the prediction errors resulting from VAE+EG+KKT, which is close to 0 and outperforms other algorithms. This shows that the proposed trajectory prediction algorithm is effective and can lead to a close-to-optimal performance, even when reducing the dimension of the communicated message by half.

We next demonstrate the value of each component in the proposed algorithm by comparing groups of benchmark algorithms.

Value of using real-time location measurement information.

We evaluate the value of integrating real-time location information into the prediction of the planned trajectories by comparing VAE and VAE+EG (Bayesian), which shows the value of adding EG. We can see from Table I that both algorithms can ensure safety and prevent collisions since the Safe-Agent Cost and Safe-Obs Cost are zero for both algorithms. We can see this in more detail in Figure 6, Figure 8 that both VAE and VAE+EG (Bayesian) can successfully keep the agent-agent and agent-obstacle distance within the desired threshold. But VAE is dangerously close in terms of agent-agent distance, making it less desirable than VAE+EG (Bayesian). Moreover, it is clear from Table I that VAE+EG (Bayesian) incurs lower costs than VAE. The same holds for prediction performance, as reflected by Tables II–IV. In summary, we can conclude that by adding the EG component, VAE+EG (Bayesian) outperforms VAE. Therefore, with the aid of the Bayesian approach, we can effectively integrate different estimations to enhance the accuracy of planned trajectories.

Value of communication. We evaluate the benefits of having the communicated message by comparing VAE+EG (Bayesian) and EG, which shows the value of having the reconstructed trajectories from VAE. Our conclusion is similar to the above analysis in that VAE+EG (Bayesian) significantly outperforms EG, as demonstrated in Tables I–IV, as well as in Figure 4 and Figures 7–8.

Value of the EvolveGCN component in considering time-varying UAV alignment. We demonstrate the value of incorporating the EvolveGCN component by comparing Baseline and EG. From Table I, Figure 4, Figure 5, and Figure 7, we can see that although Baseline outperforms EG in terms of total costs, it cannot ensure safety. It is shown in Figure 5a) and Figure 5b) that there are collisions both between UAVs and between UAVs and the obstacles, and the minimum distance is rather low. The reason is that Baseline does not produce accurate trajectory prediction outcomes, as can be seen from Tables II–IV that the prediction MSE is significantly higher than other benchmarks. This shows that the baseline may not perform well in dynamic environments where the layout of the UAV swarm constantly changes. This also shows the benefits of the EvolveGCN framework in improving safety.

Value of the KKT-informed training procedure. We evaluate the benefits of the KKT-informed training process by comparing VAE+EG+KKT with VAE+EG (Bayesian). We can see that although the prediction performance between the two benchmarks is the same (as shown in Tables II–IV), the control performance of VAE+EG+KKT is significantly better than VAE+EG (Bayesian) (as shown in Tables I, Figure 4, Figure 8, and Figure 10). This is because the KKT-informed training process enables the prediction outcome of VAE+EG+KKT to better align with the embedded QP in DMPC. This can also be reflected by comparing VAE with VAE + KKT which uses the KKT-informed component to enhance the performance of VAE, whereby the only difference is that VAE + KKT integrates a KKT-informed layer during the training procedure. We can see from Tables I, Figure 4, Figure 6, and Figure 9 that using KKT alone can enhance the performance of individual predictors. Notice that due to its high computational burden in forward propagation, we recommend using the KKT component only

in the training procedure.

Table II: Trajectory prediction accuracy (Channel 1 – x -axis)

Time Step	Base-line	EG	VAE	VAE + KKT	VAE + EG (Bayesian)	VAE + EG + KKT
1	0.41	0.34	0.18	0.09	0.07	0.07
2	0.42	0.30	0.15	0.06	0.05	0.05
3	0.51	0.28	0.14	0.05	0.05	0.05
4	0.56	0.27	0.14	0.05	0.05	0.05
5	0.64	0.26	0.14	0.06	0.05	0.05
6	0.71	0.28	0.15	0.07	0.05	0.05
7	0.77	0.28	0.17	0.08	0.06	0.06
8	0.85	0.30	0.18	0.09	0.07	0.07
9	0.91	0.32	0.19	0.10	0.08	0.08
10	0.97	0.33	0.20	0.11	0.09	0.09
11	1.02	0.35	0.22	0.12	0.10	0.09
12	1.08	0.37	0.24	0.12	0.10	0.10
13	1.14	0.38	0.25	0.13	0.10	0.10
14	1.19	0.39	0.27	0.13	0.11	0.10
15	1.25	0.40	0.28	0.19	0.11	0.10
16	1.32	0.42	0.30	0.16	0.12	0.11

Table III: Trajectory prediction accuracy (Channel 2 – y -axis)

Time Step	Base-line	EG	VAE	VAE + KKT	VAE + EG (Bayesian)	VAE + EG + KKT
1	0.15	0.02	0.03	0.01	0.01	0.02
2	0.16	0.01	0.02	0.01	0.01	0.01
3	0.18	0.01	0.02	0.01	0.01	0.01
4	0.21	0.01	0.02	0.01	0.01	0.01
5	0.24	0.01	0.02	0.01	0.01	0.01
6	0.27	0.01	0.02	0.01	0.01	0.01
7	0.31	0.01	0.02	0.01	0.01	0.01
8	0.35	0.01	0.01	0.01	0.01	0.01
9	0.39	0.01	0.01	0.01	0.01	0.01
10	0.44	0.01	0.01	0.01	0.01	0.01
11	0.48	0.01	0.01	0.01	0.01	0.01
12	0.53	0.01	0.01	0.01	0.00	0.00
13	0.57	0.01	0.01	0.01	0.00	0.00
14	0.62	0.01	0.02	0.01	0.00	0.00
15	0.67	0.01	0.02	0.01	0.01	0.01
16	0.71	0.01	0.03	0.01	0.01	0.01

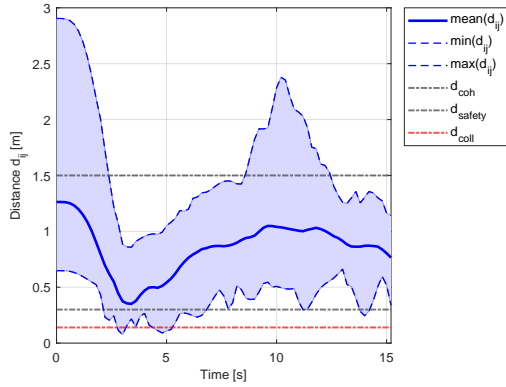
D. Robustness in scenarios with limited communication capabilities

We next demonstrate the robustness of the proposed trajectory prediction algorithm in scenarios with limited communication capabilities by evaluating the sensitivity of the proposed algorithm in these scenarios. Specifically, we evaluate the impact of trajectory compression (due to limited bandwidth, energy requirements, etc.), lower communication frequency, and packet drop on the control performance.

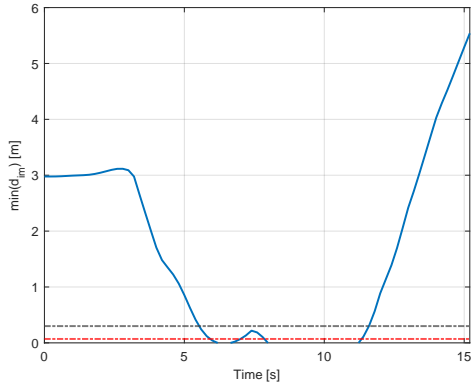
Impact of trajectory compression. We evaluate our trajectory prediction algorithm with various levels of trajectory compression, represented by the dimension of the VAE latent variable z_k (i.e., the messages exchanged between UAVs). Other parameters remain at the nominal values. Figure 12 shows the safety performance of all scenarios. Table V shows the resulting control performance, where DMPC is added as a reference. As we can see from Table V, the control performance

Table IV: Trajectory prediction accuracy (Channel 3 – z -axis)

Time Step	Base-line	EG	VAE	VAE + KKT	VAE + EG (Bayesian)	VAE + EG + KKT
1	0.24	0.02	0.03	0.03	0.03	0.03
2	0.24	0.02	0.02	0.02	0.02	0.02
3	0.25	0.03	0.03	0.03	0.02	0.02
4	0.27	0.03	0.03	0.03	0.02	0.02
5	0.29	0.03	0.03	0.03	0.01	0.01
6	0.30	0.02	0.03	0.03	0.01	0.01
7	0.32	0.02	0.02	0.02	0.01	0.01
8	0.34	0.01	0.02	0.01	0.01	0.01
9	0.37	0.01	0.02	0.02	0.01	0.01
10	0.38	0.01	0.02	0.02	0.01	0.01
11	0.41	0.01	0.02	0.01	0.01	0.01
12	0.43	0.01	0.02	0.01	0.01	0.01
13	0.45	0.01	0.02	0.01	0.01	0.01
14	0.47	0.01	0.02	0.01	0.01	0.01
15	0.50	0.01	0.03	0.01	0.02	0.02
16	0.52	0.02	0.04	0.02	0.02	0.02



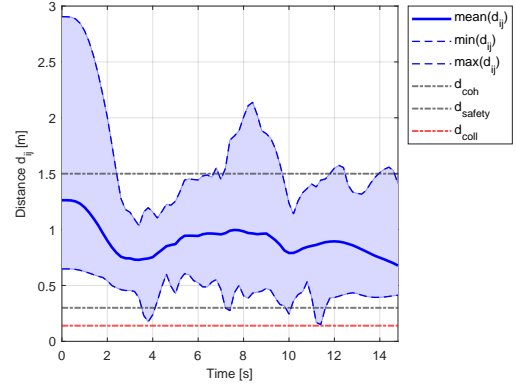
(a) Distance between UAVs



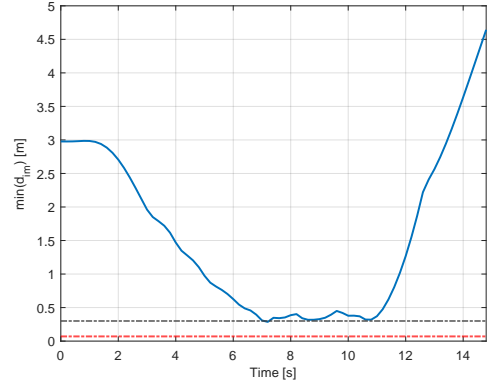
(b) Minimum distance between obstacles and UAVs

Figure 5: Evolution of distances with Baseline applied.

is close to that of DMPC as long as the latent dimension is greater than 24. For lower dimensions, although the control performance drops, the algorithm can still yield safe actions and outperform other benchmarks such as EG, VAE, and VAE+EG (Bayesian) as demonstrated in Table I. This shows that our proposed algorithm can work effectively even with low latent dimensions, suggesting that the algorithm can accommodate



(a) Distance between UAVs



(b) Minimum distance between obstacles and UAVs

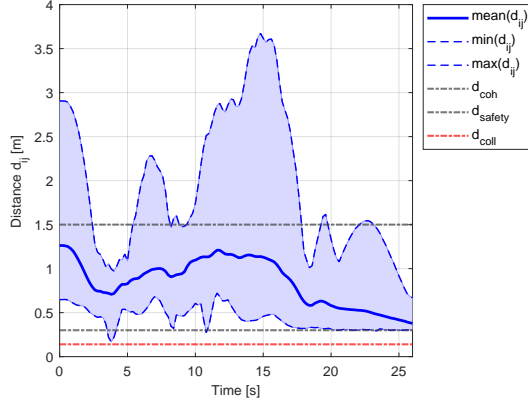
Figure 6: Evolution of distances with VAE applied.

relatively low bandwidth.

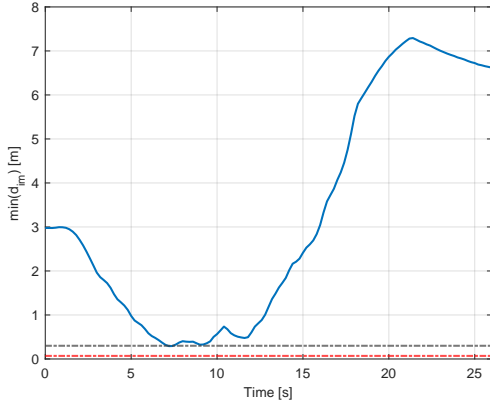
Table V: Sensitivity to the level of trajectory compression (control performance)

Latent Dim.	Safe-Agent Cost	Safe-Obs Cost	Control Effort	Cohesion Cost	Total Cost
6	0	0	165161	109800	274961
18	0	0	145297	97109	242407
24	0	0	159758	51027	210786
30	0	0	151257	53328	204585
DMPC (48)	0	0	141084	67298	208382

Impact of lower communication frequencies. We evaluate the robustness of our prediction algorithm in scenarios with various levels of communication frequencies, i.e., 1.25 Hz, 2.5 Hz, and 5 Hz, corresponding to communication every 4,2,1 time steps. Other parameters remain at the nominal values. Figure 13 shows the safety performance of all scenarios. Table VI shows the resulting control performance. As we can see from Table VI, by reducing communication frequency, the control performance drops but is still better than other benchmark algorithms such as EG and VAE. Moreover, we can see that the algorithm can still ensure safety, as the minimum distance between agents and between agents and obstacles is kept higher than the collision threshold. Therefore, we can moderately reduce the communication frequency while ensuring satisfactory control

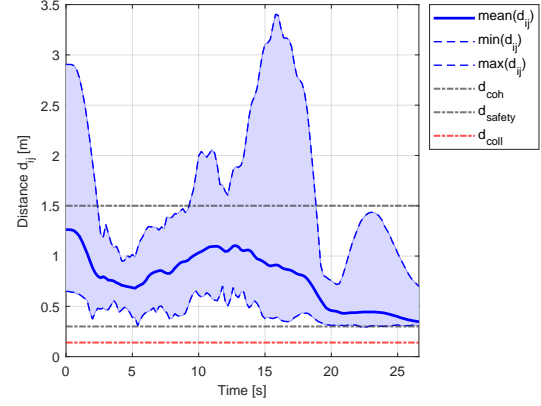


(a) Distance between UAVs

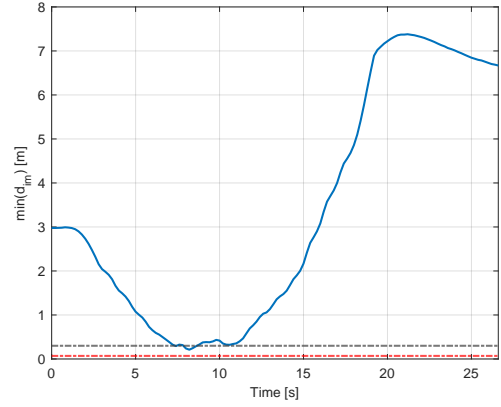


(b) Minimum distance between obstacles and UAVs

Figure 7: Evolution of distances with EG applied.



(a) Distance between UAVs



(b) Minimum distance between obstacles and UAVs

Figure 8: Evolution of distances with VAE+EG (Bayesian) applied.

performance.

Table VI: Sensitivity to communication frequencies (control performance)

Comm. Freq. (Hz)	Safe-Agent Cost	Safe-Obs Cost	Control Effort	Cohesion Cost	Total Cost
1.25	0	0	140237	156950	297188
2.5	0	0	146800	124174	270974
5	0	0	159758	51027	210786

Impact of packet loss. We evaluate the robustness of our prediction algorithm in scenarios with various packet loss probabilities (i.e., 1/2, 1/4, 1/8, 1/16). Other parameters remain at the nominal values. Figure 14 shows the safety performance of all scenarios. Table VII shows the resulting control performance. As we can see from Table VII, by increasing packet loss probabilities, the control performance drops but is still comparable with other benchmark algorithms. Note that with the same amount of communications, packet loss has a more significant impact on the control performance than reducing communication frequencies. This is because reducing communication frequencies can still lead to a well-structured communication graph that evolves according to the dynamics of UAVs, while packet loss may make the communication

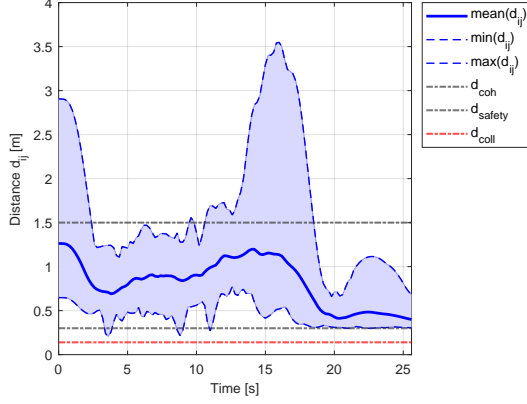
graph more random. Nevertheless, we can see from Figure 14 that the algorithm can still ensure safety.

Table VII: Sensitivity to packet loss probabilities (control performance)

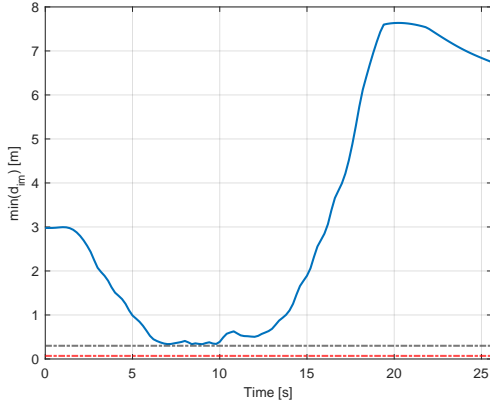
Packet loss pro.	Safe-Agent Cost	Safe-Obs Cost	Control Effort	Cohesion Cost	Total Cost
1/2	0	0	154006	159531	313537
1/4	0	0	149913	106425	256337
1/8	0	0	112363	129328	241692
1/16	0	0	165910	61686	227596
0	0	0	159758	51027	210786

E. Sensitivity to measurement noises

We evaluate the robustness of our prediction algorithm in scenarios with various measurement noises ranging from 0 to 0.032 m. Other parameters remain at the nominal values. Figure 15 shows the safety performance of all scenarios. Table VIII shows the resulting control performance. As we can see from Table VIII, the control performance drops as the magnitude of measurement noises increases. This is expected because as the quality of communication reduces, the

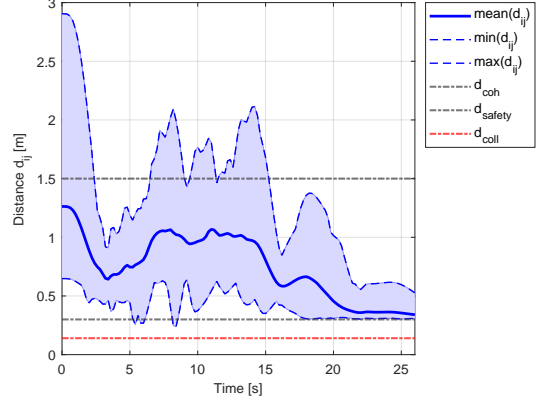


(a) Distance between UAVs

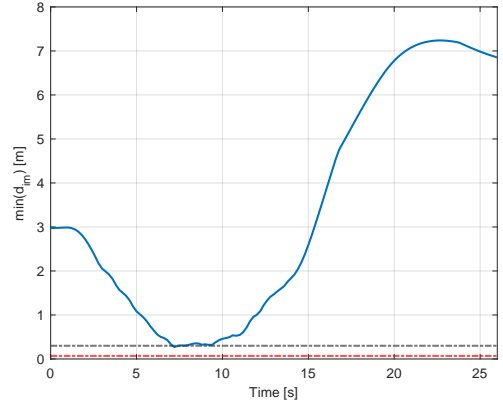


(b) Minimum distance between obstacles and UAVs

Figure 9: Evolution of distances with VAE + KKT applied.



(a) Distance between UAVs



(b) Minimum distance between obstacles and UAVs

Figure 10: Evolution of distances with VAE+EG+KKT applied.

measurement becomes more important for UAVs to sense their surroundings. Nevertheless, we can see from Figure 15 that the algorithm can still ensure safety with moderate measurement noises.

Table VIII: Sensitivity to measurement noises (control performance)

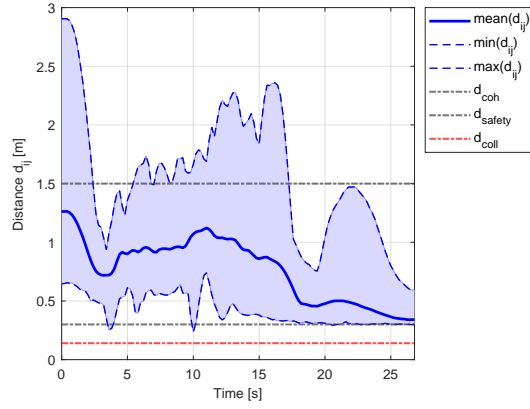
Noise Level (m)	Safe-Agent Cost	Safe-Obs Cost	Control Effort	Cohesion Cost	Total Cost
0.032	0	0	146342	148548	294889
0.024	0	0	184542	105045	289588
0.016	0	0	140848	117938	258786
0.008	0	0	158898	81059	239957
0	0	0	159758	51027	210786

V. CONCLUSION

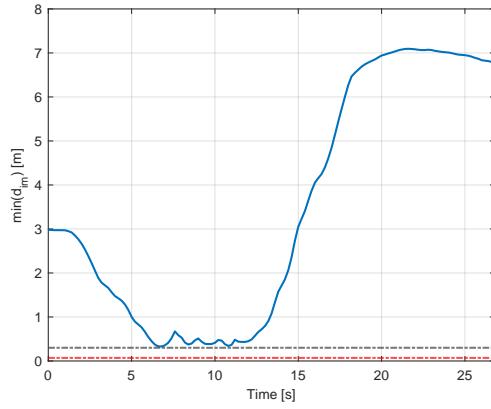
In this paper, we propose a learning-based trajectory prediction algorithm that can enable communication-efficient UAV swarm control in a cluttered environment. Specifically, our proposed algorithm can enable each UAV to predict the planned trajectories (i.e., DMPC solutions) of its neighbors in scenarios with various levels of communication capabilities. The predicted planned trajectories will serve as input to a DMPC approach with an embedded optimization problem as a

QP. The proposed algorithm involves a VAE-based trajectory compression and reconstruction model and an EvolveGCN-based trajectory prediction model, which are combined via the Bayesian formula. We further develop a KKT-informed training approach that applies the KKT conditions in the training process and thus encodes DMPC information into the trained neural network. Results show that the proposed algorithm outperforms state-of-the-art benchmarks. We have further demonstrated the value of each component of the proposed algorithm and its robustness in scenarios with limited communication capabilities and measurement noises.

This research opens several interesting directions. First, we would like to evaluate the proposed algorithm in more complex environments, e.g., with a larger swarm size and denser/less structured obstacles. Second, it would be interesting to improve the generalizability of the proposed algorithm to a broader range of possibly changing environments. One promising way of achieving this is via meta-learning or life-long learning, enabling quick adaptation and continuous updates of the proposed algorithm. Third, we would like to explicitly investigate how to encode some prior knowledge of the communication channels into the learned neural networks to better handle possible communication failures or restrictions, in order to improve the robustness of the algorithm. Fourth,



(a) Distance between UAVs



(b) Minimum distance between obstacles and UAVs

Figure 11: Evolution of distances with DMPC applied.

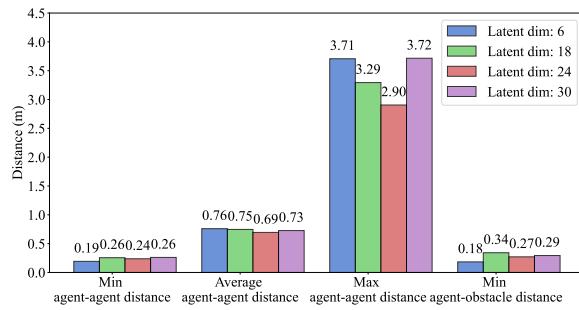


Figure 12: Sensitivity to the level of trajectory compression (safety performance)

it would be interesting to perform co-design of the trajectory prediction with communication configurations.

REFERENCES

- [1] G. Vásárhelyi, C. Virágh, G. Somorjai, T. Nepusz, A. E. Eiben, and T. Vicsek, "Optimized flocking of autonomous drones in confined environments," *Science Robotics*, vol. 3, no. 20, p. eaat3536, 2018.
- [2] M. Kamel, J. Alonso-Mora, R. Siegwart, and J. Nieto, "Robust collision avoidance for multiple micro aerial vehicles using nonlinear model predictive control," in *2017 IEEE/RSJ International Conference on Intelligent Robots and Systems (IROS)*. IEEE, 2017, pp. 236–243.

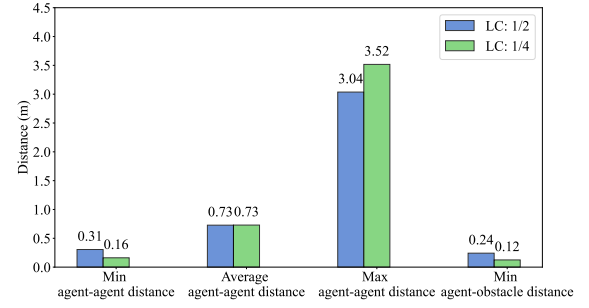


Figure 13: Sensitivity to communication frequencies (safety performance)

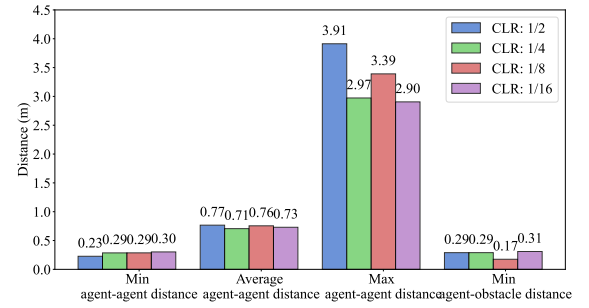


Figure 14: Sensitivity to packet loss probabilities (safety performance)

- [3] S.-J. Chung, A. A. Paranjape, P. Dames, S. Shen, and V. Kumar, "A survey on aerial swarm robotics," *IEEE Transactions on Robotics*, vol. 34, no. 4, pp. 837–855, 2018.
- [4] G. De Croon, J. Dupeyroux, S. Fuller, and J. Marshall, "Insect-inspired ai for autonomous robots," *Science Robotics*, vol. 7, no. 67, p. eabl6334, 2022.
- [5] P. Petráček, V. Walter, T. Báča, and M. Saska, "Bio-inspired compact swarms of unmanned aerial vehicles without communication and external localization," *Bioinspiration & Biomimetics*, vol. 16, no. 2, p. 026009, 2020.
- [6] E. Soria, F. Schiano, and D. Floreano, "Predictive control of aerial swarms in cluttered environments," *Nature Machine Intelligence*, vol. 3, no. 6, pp. 545–554, 2021.
- [7] A. Pareja, G. Domeniconi, J. Chen, T. Ma, T. Suzumura, H. Kanezashi, T. Kaler, T. Schardl, and C. Leiserson, "Evolvecn: Evolving graph convolutional networks for dynamic graphs," in *Proceedings of the AAAI conference on artificial intelligence*, vol. 34, no. 04, 2020, pp. 5363–5370.
- [8] H. Zhu, F. M. Claramunt, B. Brito, and J. Alonso-Mora, "Learning interaction-aware trajectory predictions for decentralized multi-robot mo-

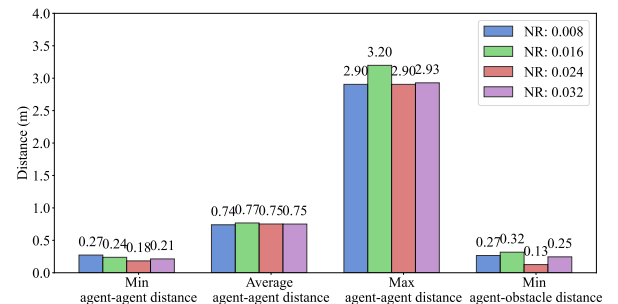


Figure 15: Sensitivity to measurement noises (safety performance)

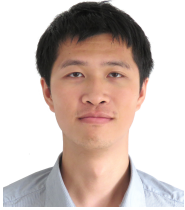
- tion planning in dynamic environments,” *IEEE Robotics and Automation Letters*, vol. 6, no. 2, pp. 2256–2263, 2021.
- [9] J. Tordesillas and J. P. How, “Mader: Trajectory planner in multiagent and dynamic environments,” *IEEE Transactions on Robotics*, vol. 38, no. 1, pp. 463–476, 2021.
 - [10] B. Amos and J. Z. Kolter, “Optnet: Differentiable optimization as a layer in neural networks,” in *International Conference on Machine Learning*. PMLR, 2017, pp. 136–145.
 - [11] Z. Wang, X. Zhou, C. Xu, and F. Gao, “Geometrically constrained trajectory optimization for multicopters,” *IEEE Transactions on Robotics*, vol. 38, no. 5, pp. 3259–3278, 2022.
 - [12] Y. Guo, C. You, C. Yin, and R. Zhang, “Uav trajectory and communication co-design: Flexible path discretization and path compression,” *IEEE Journal on Selected Areas in Communications*, vol. 39, no. 11, pp. 3506–3523, 2021.
 - [13] H. Shiri, J. Park, and M. Bennis, “Communication-efficient massive uav online path control: Federated learning meets mean-field game theory,” *IEEE Transactions on Communications*, vol. 68, no. 11, pp. 6840–6857, 2020.
 - [14] D. Chen, Q. Qi, Z. Zhuang, J. Wang, J. Liao, and Z. Han, “Mean field deep reinforcement learning for fair and efficient uav control,” *IEEE Internet of Things Journal*, vol. 8, no. 2, pp. 813–828, 2020.
 - [15] S. Zhang, H. Zhang, B. Di, and L. Song, “Cellular uav-to-x communications: Design and optimization for multi-uav networks,” *IEEE Transactions on Wireless Communications*, vol. 18, no. 2, pp. 1346–1359, 2019.
 - [16] T. Zeng, O. Semiari, W. Saad, and M. Bennis, “Joint communication and control for wireless autonomous vehicular platoon systems,” *IEEE Transactions on Communications*, vol. 67, no. 11, pp. 7907–7922, 2019.
 - [17] J. Yan, W. Cao, X. Yang, C. Chen, and X. Guan, “Communication-efficient and collision-free motion planning of underwater vehicles via integral reinforcement learning,” *IEEE Transactions on Neural Networks and Learning Systems*, 2022.
 - [18] Q.-V. Pham, M. Zeng, R. Ruby, T. Huynh-The, and W.-J. Hwang, “Uav communications for sustainable federated learning,” *IEEE Transactions on Vehicular Technology*, vol. 70, no. 4, pp. 3944–3948, 2021.
 - [19] J. Cui, Y. Liu, and A. Nallanathan, “Multi-agent reinforcement learning-based resource allocation for uav networks,” *IEEE Transactions on Wireless Communications*, vol. 19, no. 2, pp. 729–743, 2019.
 - [20] J. Kang, O. Simeone, J. Kang, and S. S. Shitz, “Joint signal and channel state information compression for the backhaul of uplink network mimo systems,” *IEEE Transactions on Wireless Communications*, vol. 13, no. 3, pp. 1555–1567, 2014.
 - [21] F. Sohrabi, T. Jiang, and W. Yu, “Learning progressive distributed compression strategies from local channel state information,” *IEEE Journal of Selected Topics in Signal Processing*, vol. 16, no. 3, pp. 573–584, 2022.
 - [22] L. Liu, S. Zhang, and R. Zhang, “Multi-beam uav communication in cellular uplink: Cooperative interference cancellation and sum-rate maximization,” *IEEE Transactions on Wireless Communications*, vol. 18, no. 10, pp. 4679–4691, 2019.
 - [23] T. Musil, M. Petrlik, and M. Saska, “Spheremap: Dynamic multi-layer graph structure for rapid safety-aware uav planning,” *IEEE Robotics and Automation Letters*, vol. 7, no. 4, pp. 11 007–11 014, 2022.
 - [24] E. Yel, S. Gao, and N. Bezzo, “Meta-learning-based proactive online planning for uavs under degraded conditions,” *IEEE Robotics and Automation Letters*, vol. 7, no. 4, pp. 10 320–10 327, 2022.
 - [25] X. Zhou, X. Wen, Z. Wang, Y. Gao, H. Li, Q. Wang, T. Yang, H. Lu, Y. Cao, C. Xu *et al.*, “Swarm of micro flying robots in the wild,” *Science Robotics*, vol. 7, no. 66, p. eabm5954, 2022.
 - [26] D. P. Kingma and M. Welling, “Auto-encoding variational bayes,” *arXiv preprint arXiv:1312.6114*, 2013.
 - [27] L. Quan, L. Yin, C. Xu, and F. Gao, “Distributed swarm trajectory optimization for formation flight in dense environments,” in *2022 International Conference on Robotics and Automation (ICRA)*. IEEE, 2022, pp. 4979–4985.
 - [28] E. Soria, F. Schiano, and D. Florean, “Distributed predictive drone swarms in cluttered environments,” *IEEE Robotics and Automation Letters*, vol. 7, no. 1, pp. 73–80, 2021.
 - [29] B. Zhou, H. Xu, and S. Shen, “Racer: Rapid collaborative exploration with a decentralized multi-uav system,” *IEEE Transactions on Robotics*, 2023.
 - [30] Z. Yu, Y. Zhang, B. Jiang, J. Fu, Y. Jin, and T. Chai, “Composite adaptive disturbance observer-based decentralized fractional-order fault-tolerant control of networked uavs,” *IEEE Transactions on Systems, Man, and Cybernetics: Systems*, vol. 52, no. 2, pp. 799–813, 2020.
 - [31] F. Ho, R. Geraldes, A. Gonçalves, B. Rigault, B. Sportich, D. Kubo, M. Cavazza, and H. Prendinger, “Decentralized multi-agent path finding for uav traffic management,” *IEEE Transactions on Intelligent Transportation Systems*, vol. 23, no. 2, pp. 997–1008, 2020.
 - [32] B. Liu, W. Ni, R. P. Liu, Y. J. Guo, and H. Zhu, “Decentralized, privacy-preserving routing of cellular-connected unmanned aerial vehicles for joint goods delivery and sensing,” *IEEE Transactions on Intelligent Transportation Systems*, 2023.
 - [33] E. Sebastián, T. Duong, N. Atanasov, E. Montijano, and C. Sagués, “Lemurs: Learning distributed multi-robot interactions,” in *2023 IEEE International Conference on Robotics and Automation (ICRA)*. IEEE, 2023, pp. 7713–7719.
 - [34] X. Liu, Y. Liu, Y. Chen, and L. Hanzo, “Trajectory design and power control for multi-uav assisted wireless networks: A machine learning approach,” *IEEE Transactions on Vehicular Technology*, vol. 68, no. 8, pp. 7957–7969, 2019.
 - [35] Z. Li, Y. Wang, and Z. Zuo, “Interaction-aware prediction for cut-in trajectories with limited observable neighboring vehicles,” *IEEE Transactions on Intelligent Vehicles*, 2023.
 - [36] K. Zhang, L. Zhao, C. Dong, L. Wu, and L. Zheng, “Ai-tp: Attention-based interaction-aware trajectory prediction for autonomous driving,” *IEEE Transactions on Intelligent Vehicles*, vol. 8, no. 1, pp. 73–83, 2022.
 - [37] J. Zhao, J. Liu, F. Gao, W. Jia, and W. Zhang, “Gridless compressed sensing based channel estimation for uav wideband communications with beam squint,” *IEEE Transactions on Vehicular Technology*, vol. 70, no. 10, pp. 10 265–10 277, 2021.
 - [38] X. Wang and M. C. Gursoy, “Learning-based uav trajectory optimization with collision avoidance and connectivity constraints,” *IEEE Transactions on Wireless Communications*, vol. 21, no. 6, pp. 4350–4363, 2021.
 - [39] Y. Wu, J. Li, Y. Xu, J.-G. Chung, Y. Dai, and Y. Xu, “Dynamic rearrangement compression algorithm for intelligent connected vehicles,” *IEEE Transactions on Vehicular Technology*, vol. 71, no. 10, pp. 10 350–10 360, 2022.
 - [40] H. Dong, J. Yu, Y. Xu, Z. Xu, Z. Shen, J. Tang, Y. Shen, and Y. Wang, “Mr-gmmapping: Communication efficient multi-robot mapping system via gaussian mixture model,” *IEEE Robotics and Automation Letters*, vol. 7, no. 2, pp. 3294–3301, 2022.
 - [41] K. McGuire, C. De Wagter, K. Tuyls, H. Kappen, and G. C. de Croon, “Minimal navigation solution for a swarm of tiny flying robots to explore an unknown environment,” *Science Robotics*, vol. 4, no. 35, p. eaaw9710, 2019.
 - [42] Y. Wang, X. Wen, Y. Cao, C. Xu, and F. Gao, “Bearing-based relative localization for robotic swarm with partially mutual observations,” *IEEE Robotics and Automation Letters*, vol. 8, no. 4, pp. 2142–2149, 2023.
 - [43] A. Brandstätter, S. A. Smolka, S. D. Stoller, A. Tiwari, and R. Grosu, “Multi-agent spatial predictive control with application to drone flocking,” in *2023 IEEE International Conference on Robotics and Automation (ICRA)*. IEEE, 2023, pp. 1221–1227.
 - [44] C. E. Luis, M. Vukosavljev, and A. P. Schoellig, “Online trajectory generation with distributed model predictive control for multi-robot motion planning,” *IEEE Robotics and Automation Letters*, vol. 5, no. 2, pp. 604–611, 2020.
 - [45] X. Fan, P. Wu, and M. Xia, “Air-to-ground communications beyond 5g: Uav swarm formation control and tracking,” *IEEE Transactions on Wireless Communications*, 2024.
 - [46] S. Huang, H. Zhang, and Z. Huang, “E²copre: Energy efficient and cooperative collision avoidance for uav swarms with trajectory prediction,” *IEEE Transactions on Intelligent Transportation Systems*, 2024.



Longhao Yan receives the B.Eng. degree and M.Eng. degree in School of Electronics and Control Engineering from Chang'an University, Xi'an, China, in 2019 and 2022 respectively. He is currently working towards a Ph.D. degree with the National University of Singapore. His research interests include lateral control and trajectory prediction of intelligent transportation system.



Jingyuan Zhou receives the B.Eng. degree in Electronic Information Science and Technology from Sun Yat-sen University, Guangzhou, China, in 2022. He is currently working towards a Ph.D. degree with the National University of Singapore. His research interests include safety-critical control and privacy computing of mixed-autonomy traffic.



Kaidi Yang is an Assistant Professor in the Department of Civil and Environmental Engineering at the National University of Singapore. Prior to this, he was a postdoctoral researcher with the Autonomous Systems Lab at Stanford University. He obtained a PhD degree from ETH Zurich and M.Sc. and B.Eng. degrees from Tsinghua University. His main research interest is the operation of future mobility systems enabled by connected and automated vehicles (CAVs) and shared mobility.